

Triggering hallucinations in model-based MRI reconstruction via adversarial perturbations

Suna Buğday¹, Yvan Saeys^{2,3}, and Jonathan Peck^{2,3*}

¹ Faculty of Engineering and Architecture/Computer Engineering, İzmir Bakırçay University, İzmir, Turkey

² Department of Computer Science, Mathematics and Statistics, Ghent University, Ghent, Belgium

³ Data Mining and Modeling for Biomedicine Group, VIB Inflammation Research Center, Ghent, Belgium

Abstract. Generative models are increasingly used to improve the quality of medical imaging, such as reconstruction of magnetic resonance images and computed tomography. However, it is well-known that such models are susceptible to *hallucinations*: they may insert features into the reconstructed image which are not actually present in the original image. In a medical setting, such hallucinations may endanger patient health as they can lead to incorrect diagnoses. In this work, we aim to quantify the extent to which state-of-the-art generative models suffer from hallucinations in the context of magnetic resonance image reconstruction. Specifically, we craft adversarial perturbations resembling random noise for the unprocessed input images which induce hallucinations when reconstructed using a generative model. We perform this evaluation on the brain and knee images from the fastMRI data set using UNet and end-to-end VarNet architectures to reconstruct the images. Our results show that these models are highly susceptible to small perturbations and can be easily coaxed into producing hallucinations. This fragility may partially explain why hallucinations occur in the first place and suggests that a carefully constructed adversarial training routine may reduce their prevalence. Moreover, these hallucinations cannot be reliably detected using traditional image quality metrics. Novel approaches will therefore need to be developed to detect when hallucinations have occurred.

Keywords: deep learning · computer vision · magnetic resonance imaging · robustness

1 Introduction

When patients go in for a medical scan, such as magnetic resonance imaging (MRI) or computed tomography (CT), the resulting images must first be cleaned up or *reconstructed* before they can be used for diagnostic purposes. There are

* Corresponding author: Jonathan.Peck@UGent.be

multiple reasons for this: patients never stay completely still during scans, which causes blurring; the physical measurement process is subject to thermal noise and electromagnetic interference; etc [7]. Scanners also frequently undersample or *accelerate* their measurements, which can lead to aliasing and other artifacts due to incomplete data [30]. For MRI, acceleration is usually performed to save costs and to increase patient comfort: a fully-sampled MRI would take several hours compared to the few minutes patients typically spend inside such a scanner in practice [5]. For CT, minimizing the acquisition time is actually a necessity due to the exposure to a radioactive isotope which can damage tissues over an extended period of time.

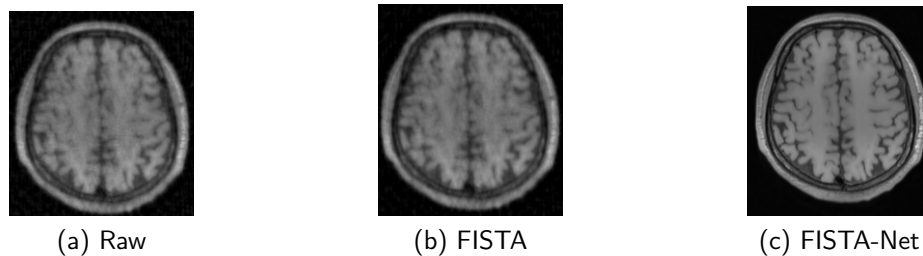


Fig. 1. Comparison of classical FISTA and model-based FISTA-Net reconstruction of brain MR images. These images were taken from [3].

Naturally, there is a long line of research into proper ways of reconstructing medical imaging data [6, 12, 32, 42]. These “classical” algorithms are based on mathematical optimization problems and have attractive theoretical guarantees, such as convergence rates and bounds on the reconstruction error. More recently, the use of neural networks to reconstruct medical imaging data has been explored [1, 3, 29, 46]. Several studies have confirmed that the resulting reconstructions are more visually appealing than those generated by classical algorithms [37, 38]. As an example, figure 1 compares the classical FISTA algorithm [6] to the more recent model-based FISTA-Net method [3]. The improvement in visual quality is obvious here.

Nevertheless, generative neural networks typically lack theoretical guarantees, calling their reliability in this context into question [28, 45]. Empirically, it is known that generative models of any kind are susceptible to so-called *hallucinations*. Hallucinations occur when a generative model adds an important feature to its output that was not supposed to be there, or removes a feature that should have been present. This problem is particularly well-known in the field of language modeling: modern large language models (LLMs) are notoriously prone to generating convincing misinformation or outright nonsense [24, 55]. However, imaging models are not exempt from this problem: a few examples are shown in figure 2. These alterations can have a significant impact on patient care. As such, it is an important open problem to detect when such hallucinations may

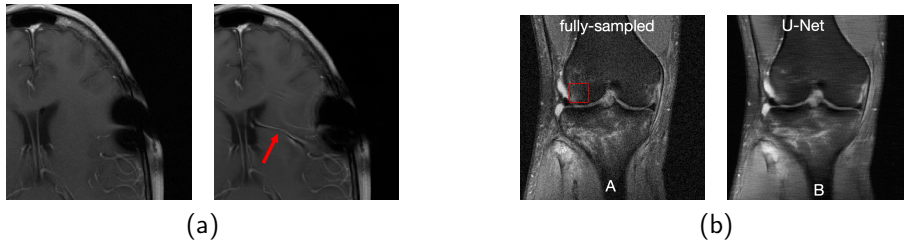


Fig. 2. Examples of hallucinations introduced by model-based reconstructions of MR images. (a) In this image from [37], the model-based reconstruction introduces an additional sulcus in the brain which was not present in the original. (b) In this image taken from [18], the model-based reconstruction removes evidence of a meniscal tear that is present in the original data.

have occurred and to prevent them from happening if possible. Currently, there are no effective methods to address these issues [30].

In this work, we aim to contribute towards effective mitigation of hallucinations in medical imaging by crafting an algorithm which actively *provokes* them in state-of-the-art model-based reconstructions. Our motivation is that such an algorithm would facilitate follow-up research into the detection and mitigation of hallucinations. For instance, the algorithm could be used to create a data set of reconstructions containing hallucinations. Combined with clean reconstructions, a training data set can be created to train a detector that flags hallucinations. Alternatively, the algorithm could also serve as a component in an adversarial training regime that improves the robustness of generative models such that hallucinations occur less frequently.

We evaluate our attack on the fastMRI data set [56] against UNet [43] and E2E-VarNet [46] models, which have been found to obtain good performance on these reconstruction tasks. Our attack seems to be highly successful at eliciting hallucinations via imperceptibly small perturbations of the input, leading to the conclusion that these models are highly unstable and hallucinations can easily arise in practice purely as a result of noise. We perform further experiments to attempt to detect the hallucinations using standard image quality metrics, such as peak signal-to-noise ratio (PSNR), normalized root mean squared error (NRMSE) and structural similarity index (SSIM; [53]). We find that the distributions of these metrics overlap almost completely and hence cannot be used to distinguish reliable reconstructions from those containing hallucinations. The code to reproduce our experiments is available at <https://github.com/saeyslab/adversarial-mri>.

2 Background

Many imaging reconstruction problems are essentially instances of a particular *linear inverse problem* [41, 51]. Formally, we observe some noisy vector $\mathbf{y} \in \mathbb{C}^m$

which is assumed to be produced according to a so-called *forward model*:

$$\mathbf{y} = \Phi \cdot \mathbf{x}^{\natural} + \mathbf{e}. \quad (1)$$

Here, $\mathbf{x}^{\natural} \in \mathbb{C}^n$ is the true signal, $\Phi \in \mathbb{C}^{m \times n}$ is a measurement matrix (also referred to as the *forward transform*) and $\mathbf{e} \in \mathbb{C}^m$ is noise. We always have $m < n$, so the original signal \mathbf{x}^{\natural} is subject to both compression (via Φ) and additive noise (given by \mathbf{e}). The goal is to reconstruct \mathbf{x}^{\natural} as faithfully as possible given the noisy and compressed observations \mathbf{y} .

MRI and CT scans present typical examples of linear inverse problems. In CT, the observations \mathbf{y} are sinograms obtained via X-ray projections of the original image \mathbf{x}^{\natural} from various directions [57]. In the case of MRI, the observations are spatial frequencies in Fourier space, referred to as *k-space* in the literature [30]. Mathematically, the measurement matrices of CT and MRI are given by the discrete Radon transform [8] and discrete Fourier transform [54], respectively.

The solutions to linear inverse problems are typically obtained via iterative optimization procedures based on a probabilistic model of the noise and the forward transform. The conditional density $p_{\mathbf{Y}|\mathbf{X}}(\mathbf{y} | \mathbf{x})$ is usually known from the physics of the measurement process. The most common choice is to assume Gaussian noise, so that \mathbf{y} is normally distributed around $\Phi \cdot \mathbf{x}^{\natural}$. This leads to an optimization problem known as *basis pursuit* [16]:

$$\hat{\mathbf{x}} = \arg \min_{\mathbf{x} \in \mathbb{C}^n} \frac{1}{2} \|\mathbf{y} - \Phi \cdot \mathbf{x}\|_2^2 + \lambda \mathcal{R}(\mathbf{x}). \quad (2)$$

The L_2 penalty is referred to as the *data consistency objective* and is a direct result of the Gaussian assumption on \mathbf{e} . The second term, $\mathcal{R}(\mathbf{x})$, is a regularizer which depends on the choice of prior $p_{\mathbf{X}}(\mathbf{x})$. Common choices for \mathcal{R} include the L_1 norm in image space, $\|\mathbf{x}\|_1$; the L_1 norm in wavelet space, $\|\Psi \cdot \mathbf{x}\|_1$, where Ψ is a discrete wavelet transform [49]; or the total variation of \mathbf{x} [14]. The resulting reconstruction algorithms are well-documented in various surveys and textbooks [25].

2.1 Model-based reconstruction

The success of deep learning approaches in the image domain suggests that deep neural networks may have potential in determining good solutions to linear inverse problems for medical imaging. While it is possible to train a neural network to directly learn the mapping from the observation space to the original image space [29], this strategy poses the risk of hallucinations [9, 28, 30] and lacks formal guarantees on the reconstruction quality. In particular, when a neural network is used to reconstruct the image directly, it is not clear what the underlying inverse problem actually is that is being solved, which casts doubt on the reliability of the results [45].

In light of these issues, some authors have attempted to use deep networks as a regularizer rather than a full reconstruction algorithm. Specifically, they retain the original optimization problem (2) but incorporate the neural network into

the regularizer $\mathcal{R}(\mathbf{x})$. This is the approach taken by the MoDL framework [1], which reconstructs the image by solving (2) with

$$\mathcal{R}(\mathbf{x}) = \|\mathbf{x} - F_\theta(\mathbf{x})\|_2^2,$$

where F_θ is a trained denoising neural network. In this case, the regularization consists of minimizing the estimated noise in the image as determined by a neural network reconstruction.

2.2 Adversarial perturbations

Adversarial perturbations are worst-case alterations of the inputs to a machine learning model, in the sense that they are intended to be imperceptible or harmless to a human observer while causing models to make mistakes [48]. In the image domain, they typically take the form of (nearly) imperceptible distortions. For discriminative models, the goal of adversarial perturbations is usually to cause misclassification. In the case of generative models, performance is generally harder to quantify but usually relies on minimizing some measure of similarity between the output of the model and a reference. Examples include the mean squared error (MSE) or the structural similarity index measure (SSIM) [53].

Adversarial perturbations have been the subject of much research for a long time now [10, 11], and while certain promising defenses have been proposed, the problem is still far from being considered “solved” in any meaningful way [21, 40]. In this work, we will make use of adversarial perturbations to craft imperceptible distortions that, when added to an MR image, result in hallucinations when reconstructed by a neural network.

2.3 Related work

Adversarial perturbations for medical images are not new, and many attacks and defenses have been proposed to date [23, 31]. However, the vast majority of existing work focuses on classification tasks, which is the most straightforward setting for an adversarial attack because success is easy to measure through misclassification rate. By contrast, we focus here on attacking *reconstruction* tasks, which is a generative setting where the objective is to remove undesirable artifacts from the data and improve visual quality.

In this vein, [22] also consider the UNet and E2E-VarNet models we study here and compare their robustness to classical methods such as total variation (TV) minimization. They find that *both* neural networks as well as classical reconstruction algorithms are vulnerable to adversarial perturbations specifically tailored to the methods in question. This finding seems to contradict other studies such as [26] who claim that TV minimization is provably robust. In fact, [26] further find that neural networks are resilient against adversarial perturbations, which also contradicts our own results. Although the existing body of work on robustness of image reconstruction seems to favor the view that classical reconstruction algorithms are stable whereas neural networks are not, consensus on this question does not seem to have been reached yet.

Theoretical results on the stability of classical reconstruction algorithms have been obtained by [2]. From their work, we can conclude that classical methods should not suffer from the same instability with respect to small perturbations, given the favorable continuity properties these methods enjoy. [20] prove several results related to the (non-)existence of accurate and stable neural networks for inverse problems. They also introduce FIRENETs, a family of neural networks that can be efficiently trained and have provable stability properties. More recently, [28] related the instabilities of model-based reconstruction methods to the kernel of the measurement matrix. Their main results are broadly applicable to many reconstruction algorithms (not merely neural networks), and consist of a few “no free lunch” theorems which show that (paradoxically) higher performance increases the probability of hallucination, and that hallucinations are not rare events (in the sense of having non-zero probability of occurring).

The work that comes closest to ours is [36], who also study adversarial perturbations for MRI reconstruction. They evaluate adversarial attacks against UNet [43] and E2E-VarNet [46] on the fastMRI data set [56]. These attacks are untargeted in the sense that they aim to maximize the reconstruction error within a specified region with respect to fully sampled reference images. By contrast, in this work, we study a targeted adversarial attack which aims to insert a specific detail into the reconstruction that is not actually present. This attack requires no reference data and supports any type of detail which can be efficiently rendered onto an image. We also perform additional experiments in an attempt to detect the hallucinations we inserted using standard image quality metrics, such as PSNR, NRMSE and SSIM, and find that these are ineffective.

3 Method

The goal of our attack is to craft invisible perturbations such that model-based reconstructions of the perturbed data points exhibit distortions that could mislead diagnostic interpretation. To achieve this, given a k -space data vector $\mathbf{z} \in \mathbb{C}^n$ and a reconstruction map $F : \mathbb{C}^n \rightarrow \mathbb{R}^n$, we solve the following optimization problem:

$$\boldsymbol{\delta}^* = \arg \min_{\boldsymbol{\delta} \in \mathbb{C}^n} \frac{\|\mathbf{m} \odot (F(\mathbf{z} + \boldsymbol{\delta}) - \mathbf{y}_t)\|_2^2}{\|\mathbf{m}\|_1} + \frac{\|(1 - \mathbf{m}) \odot (F(\mathbf{z} + \boldsymbol{\delta}) - F(\mathbf{z}))\|_2^2}{\|1 - \mathbf{m}\|_1} \quad (3)$$

subject to the constraint $\|\boldsymbol{\delta}\|_\infty \leq \varepsilon$, where $\varepsilon > 0$ is the perturbation budget, $\mathbf{m} \in \mathbb{R}^n$ is a binary mask, and \mathbf{y}_t is a target reconstruction.

The budget ε must be sufficiently small so that the generated perturbations are invisible to the naked eye, but large enough to allow insertion of the desired hallucinations in the reconstruction. The specific value therefore depends on the application; see section 4 for further details.

The target reconstruction \mathbf{y}_t is designed by drawing a short white line in the center of the original reconstruction $F(\mathbf{z})$. The mask \mathbf{m} delimits the region

where this line was added. In this way, the objective function in (3) strikes a balance between the insertion of the specified detail on the one hand and faithful reconstruction of the image on the other: the first term in the loss penalizes the difference between the reconstruction and the target image, whereas the second term penalizes the difference between the reconstruction and the ground truth. The optimal solution is achieved when the perturbation δ is such that $F(\mathbf{z} + \delta)$ is identical to \mathbf{y}_t within the target region defined by the mask \mathbf{m} and identical to $F(\mathbf{z})$ outside the target region.

Pseudocode describing the attack is provided in appendix A. The method is inspired by the basic iterative method (BIM), which is a popular algorithm for generating adversarial examples [33]. Note that k -space data is complex-valued, but we consider only real-valued perturbations δ in our algorithm. This is done to simplify the computations on the one hand, but also because we noticed that, for our purposes, it suffices to only perturb the real components of the k -space vector. Hence we leave the imaginary components of all samples unchanged.

Although in this work we only consider lines drawn onto the center of the image, the attack we developed here is agnostic to the specific target. Indeed, the attack can use any target \mathbf{y}_t with associated mask \mathbf{m} and hence can be used to provoke all kinds of hallucinations, as long as they can be efficiently rendered onto an image. We chose lines here because they are simple yet already highly effective at introducing unwanted artifacts, but other shapes such as squares or circles may also be used. An interesting further experiment could be to use parts of other images, which include real pathologies, and render them onto images which do not contain them. In this way, a convincing meniscal tear might be hallucinated onto an image of a healthy knee, for instance. This can be facilitated using annotations of pathologies in existing MRI data sets, such as fastMRI+.⁴

4 Experiments

We evaluated our attack algorithm on the fastMRI data set [56] using a pre-trained UNet [43] and E2E-VarNet [46]. We consider single-coil and multi-coil knee images, as well as multi-coil brain images. We do not evaluate E2E-VarNet on the single-coil knee images, since there were no pretrained checkpoints available for that model on this part of the fastMRI data set. The adversarial perturbations are generated by solving (3) using algorithm A.1 with $T = 150$ iterations. The magnitude of the perturbation was bounded in the L_∞ norm to a maximum of $\varepsilon = 1 \times 10^{-6}$ with a step size of $\alpha = 1 \times 10^{-7}$.

4.1 Results

We performed a quantitative evaluation of the results using peak signal-to-noise ratio (PSNR), normalized root mean squared error (NRMSE), and structural similarity index measure (SSIM). These metrics are computed separately for the

⁴ <https://github.com/microsoft/fastmri-plus>

pairs of original and perturbed input samples, as well as the pair of original and perturbed reconstructions. We also investigated the value of the objective function in (3) and found that it was almost always negligibly small across all models and data sets (on the order of 10^{-8} or less). We therefore do not include these values in the report, but we conclude that they are indicative of a successful attack.

Table 1. Summary statistics of the experiments. The reported numbers are means over the entire data set along with their standard deviations in parentheses.

Model	Data	PSNR \uparrow	NRMSE \downarrow	SSIM \uparrow
UNet	sc-knee	55.60 (6.18)	0.01 (0.01)	1.00 (0.00)
		34.24 (10.10)	0.17 (0.33)	0.95 (0.10)
	mc-knee	50.35 (5.74)	0.02 (0.01)	1.00 (0.00)
		28.48 (4.62)	0.23 (0.13)	0.82 (0.13)
	mc-brain	61.72 (4.58)	0.01 (0.00)	1.00 (0.00)
		26.00 (11.06)	0.76 (1.07)	0.68 (0.34)
VarNet	mc-knee	50.69 (6.24)	0.02 (0.01)	1.00 (0.01)
		31.70 (1.70)	0.42 (0.18)	0.93 (0.03)
	mc-brain	60.10 (4.44)	0.01 (0.00)	1.00 (0.00)
		41.72 (7.48)	0.10 (0.10)	0.98 (0.03)

Summary statistics of these metrics are given in table 1, with values rounded to two decimal places. For every metric $M \in \{\text{PSNR}, \text{NRMSE}, \text{SSIM}\}$, we report the mean and standard deviation of two values across the data set:

1. The metric computed on the zero-filled⁵ original and adversarial input samples, $M(\text{ZF}(\mathbf{z}), \text{ZF}(\mathbf{z} + \boldsymbol{\delta}))$, where $\text{ZF}(\cdot)$ denotes the zero-filling operation.
2. The metric computed on the reconstructions, $M(F(\mathbf{z}), F(\mathbf{z} + \boldsymbol{\delta}))$.

We report these two values for each metric to gauge the success of the attack: in each case, we expect the metric computed on the zero-filled pair to be “good” – high in the case of PSNR and SSIM, low for NRMSE – but the reconstructions should be noticeably worse. We do indeed observe this pattern in table 1: the metric values are consistently better for the zero-filled originals compared to the reconstructions. For the originals, PSNR values are always at least 50 dB, the NRMSE is 0.02 or less and the SSIM is almost 100%. This suggests that the clean input samples and the adversarial samples are visually indistinguishable, as desired. On the other hand, the metric values for the reconstructed samples are noticeably worse: PSNR values drop to around 40 dB or less, NRMSE increases by at least an order of magnitude and SSIM values can drop up to thirty

⁵ Zero-filling is the most basic reconstruction method where we simply apply an inverse Fourier transform on the raw k -space data (possibly padded with additional zeros), without making any attempt at reducing noise.

percentage points. Although these values still indicate that the reconstructions are similar, there is a significant difference. Moreover, it is expected for the reconstructions to retain much similarity, because the artificial detail we added using our adversarial attack only covers a small portion of the image.

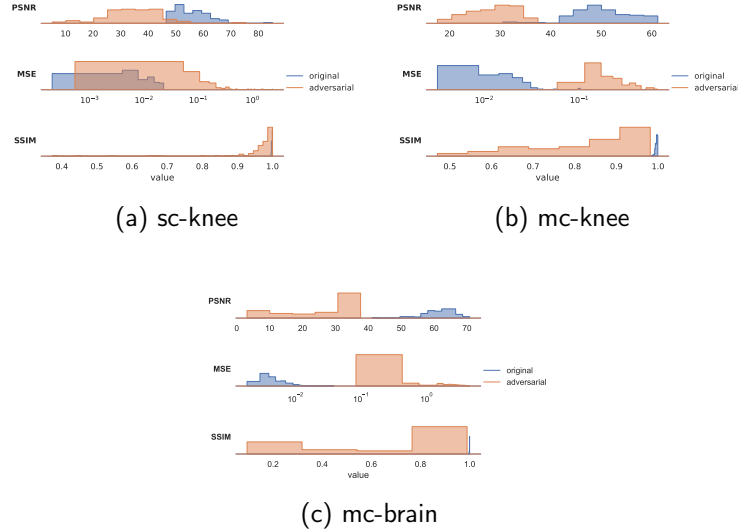


Fig. 3. Distributions of the metric values for the UNet model.

To further investigate the extent to which our attack can be called successful, we plot the full distributions of the metric values in figure 3 for the UNet model and figure 4 for the VarNet model. These values are visualized as histogram-based ridge plots, showing the overlap between the distributions. Note that the MSE values are shown on a semi-logarithmic scale.

Consistent with table 1, we observe that the distributions of all metric values tend to be well-separated between the original samples and the reconstructions. Some exceptions to this can be observed: the distributions of NRMSE for the sc-knee data reconstructed by the UNet model largely overlap, as do the distributions of SSIM values for the sc-knee data reconstructed by the UNet model and mc-brain data reconstructed by the E2E-VarNet model. In all of these cases, however, we observe that the metrics involved have a significantly larger spread after reconstruction. This indicates that the hallucinated details may not always be very visible, but given the large variance in the values, the attack is still very likely to produce noticeable distortions for the majority of inputs.

A qualitative assessment of the generated images was also performed but has been deferred to appendix B due to space constraints. From those results,

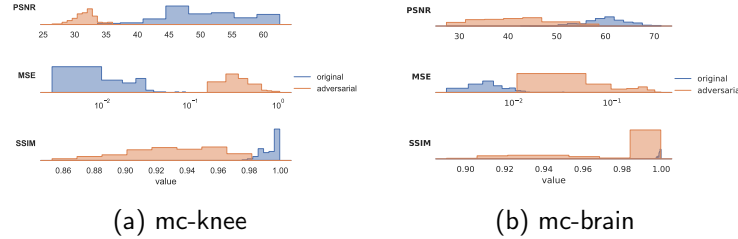


Fig. 4. Distributions of the metric values for the E2E-VarNet model.

we conclude that the adversarially perturbed samples can lead to realistic reconstructions which exhibit biologically plausible distortions that could mislead expert interpretation, and that the insertion of the artificial detail will often cause further distortion far beyond the target region delineated by our mask.

4.2 Detecting hallucinations

In this section, we turn to the question of detectability of our generated hallucinations. We consider a simple threat model where an adversary may have contaminated part of a data set using perturbations generated by algorithm A.1. The defender is given access only to k -space vectors $\mathbf{z}_1, \dots, \mathbf{z}_N$ and must decide which (if any) of the samples have been corrupted.

As argued above, it is expected that classical reconstruction algorithms such as total variation, conjugate gradients and FISTA do not suffer from hallucinations. It therefore stands to reason that such algorithms may be used to compute an expected distribution of residual reconstruction errors against which we may test the model-based reconstructions. Specifically, given a potentially perturbed k -space vector \mathbf{z} , we ask whether it is possible to detect hallucinations using standard image quality metrics applied to the pair $R(\mathbf{z})$ and $F(\mathbf{z})$, where $R(\cdot)$ denotes some classical reconstruction algorithm.

We test this hypothesis by first using algorithm A.1 to generate a data set of perturbed k -space vectors $\tilde{\mathbf{z}}_1, \dots, \tilde{\mathbf{z}}_N$. Then, for each unperturbed k -space vector \mathbf{z} and its adversarially perturbed counterpart $\tilde{\mathbf{z}}$, we compute PSNR, NRMSE and SSIM metrics on the pairs of reconstructions $(\text{TV}(\mathbf{z}), F(\mathbf{z}))$ and $(\text{TV}(\tilde{\mathbf{z}}), F(\tilde{\mathbf{z}}))$, where $\text{TV}(\cdot)$ is the total variation reconstruction algorithm as implemented in the SigPy library⁶ using sensitivity maps estimated by ESPiRiT [52]. If these distributions are well-separated, then the defender can simply compute these metrics for each sample in the data set and compare them to a pre-determined threshold.

The distributions of the resulting values are given in figure 5 for the UNet model and figure 6 for the E2E-VarNet model. From these results we observe

⁶ <https://github.com/mikgroup/sigpy>

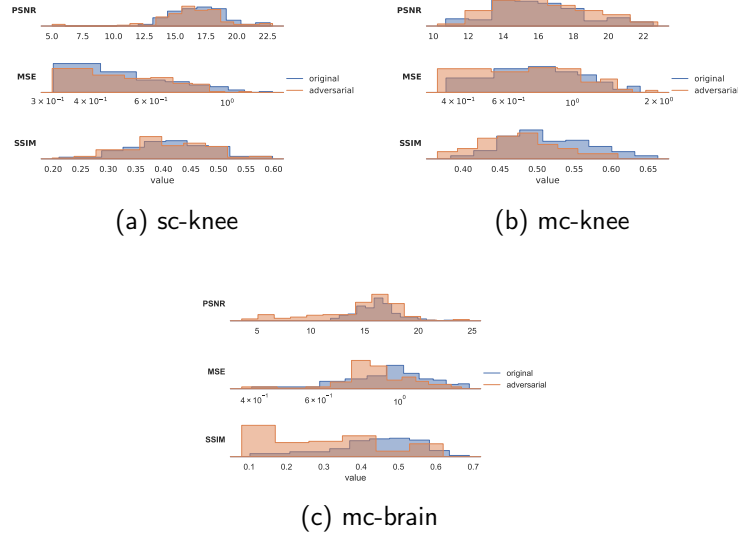


Fig. 5. Distributions of the metric values for the UNet model using total variation reconstructions.

that, for every metric, the two distributions almost entirely overlap. The only exception seems to be the SSIM metric on the mc-brain data for the UNet model, which exhibits an unusual peak near 10%. However, this pattern never repeats for any of the other data sets and does not appear at all for the E2E-VarNet model. It therefore seems unreliable, and the distributions still overlap sufficiently to make any attempt at separation using the SSIM prone to error.

We stress that algorithm A.1 was not explicitly constructed to maximize overlap between these metrics. Indeed, our attack merely minimizes (3) and does not make any use of other reconstruction algorithms, nor does it directly optimize PSNR or SSIM. Yet it appears this approach already suffices to make the generated hallucinations essentially undetectable using standard image quality metrics. As is common practice in adversarial attacks [50], algorithm A.1 may be extended by including such additional objectives into the loss function in order to make the perturbations even less detectable, but it seems this is not necessary here.

Note that we do not explore the possibility of training model-based detectors for these perturbations here. This omission is due to our expectation that such approaches are bound to be ineffective, since the field of adversarial machine learning has learned through experience [4, 13, 40, 50] that adversarial attacks can be easily adapted to incorporate the outputs of such detectors. Hence, an evaluation where we train a neural network to differentiate between clean and

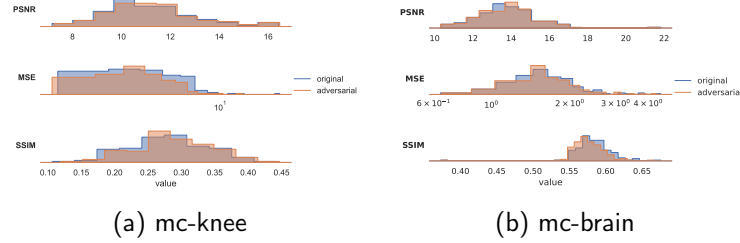


Fig. 6. Distributions of the metric values for the E2E-VarNet model using total variation reconstructions.

perturbed k -space vectors would merely serve to create a false sense of security, and would likely result in a swift break of the detector in a follow-up work.

These findings suggest that, in order to solve the problem of hallucinations in model-based MRI reconstructions, mathematically principled approaches will be needed that give rise to *certified* defenses or detectors. In this vein, carefully constructed adversarial training regimes [34, 35] or the application of denoised smoothing [19, 44] may be explored.

5 Conclusions

We have proposed an adversarial attack which can insert hallucinations into model-based MRI reconstructions via invisible perturbations of the input samples. We evaluated the algorithm using several image quality metrics and found that it often succeeds in causing significant distortion of the reconstructed samples while remaining invisible to the naked eye in input space. Our results imply that, in the absence of reference data, such distortions are not easily detected using “traditional” metrics such as peak signal-to-noise ratio, mean squared error or structural similarity index. Moreover, a qualitative assessment of the results indicates that whenever our attack is successful, it tends to cause further biologically plausible distortions beyond the neighborhood of the artificially inserted detail.

We conclude that state-of-the-art model-based MRI reconstruction algorithms are highly unstable with respect to small noise and can easily be induced to insert hallucinatory structures. This poses a risk when these models are used in medical contexts, where such perturbations may arise spontaneously through noise and may affect diagnosis and eventual treatment of patients. Future work in this area should focus on reducing the instability of reconstruction maps to small perturbations as well as developing detection mechanisms which can signal when reconstructions may be unreliable. The attack introduced in this work may form the basis for an adversarial training regime that could improve the robust-

ness of model-based MRI reconstruction or serve as a baseline against which to benchmark potential detection approaches.

Given the historical failure of many approaches to detecting adversarial perturbations, we argue that future research in this direction should focus on mathematically principled techniques that lead to detectors with provable correctness even in the presence of worst-case perturbations. It is known that detecting adversarial perturbations is a very hard problem in general, and no satisfying general-purpose solutions exist at this time [11,40]. However, when the problem is constrained specifically to the detection of hallucinations in MRI reconstruction, existing mathematical results in compressed sensing may be employed which are not available in more general settings [17,39,47]. It is our hope that this may lead to provable solutions to the problem of hallucinations in model-based MRI reconstruction.

Acknowledgments. Suna Buğday was supported by an Erasmus+ mobility grant during her stay at Ghent University.

References

1. Aggarwal, H.K., Mani, M.P., Jacob, M.: MoDL: Model-based deep learning architecture for inverse problems. *IEEE transactions on medical imaging* **38**(2), 394–405 (2018)
2. del Aguila Pla, P., Neumayer, S., Unser, M.: Stability of image-reconstruction algorithms. *IEEE Transactions on Computational Imaging* **9**, 1–12 (2023)
3. Aromal, C., Datta, S.: FISTA-NET: Compressed sensing MRI reconstruction using unrolled iterative networks. In: 2024 IEEE 21st India Council International Conference (INDICON). pp. 1–6. IEEE (2024)
4. Athalye, A., Carlini, N., Wagner, D.: Obfuscated gradients give a false sense of security: Circumventing defenses to adversarial examples. In: International conference on machine learning. pp. 274–283. PMLR (2018)
5. Ballinger, J., Wilczek, M., Knipe, H.: Acquisition time (Apr 2013). <https://doi.org/10.53347/rid-22553>, <http://dx.doi.org/10.53347/rid-22553>
6. Beck, A., Teboulle, M.: A fast iterative shrinkage-thresholding algorithm for linear inverse problems. *SIAM journal on imaging sciences* **2**(1), 183–202 (2009)
7. Bellon, E.M., Haacke, E.M., Coleman, P.E., Sacco, D.C., Steiger, D.A., Gangarosa, R.E.: MR artifacts: a review. *American Journal of Roentgenology* **147**(6), 1271–1281 (1986)
8. Beylkin, G.: Discrete Radon transform. *IEEE transactions on acoustics, speech, and signal processing* **35**(2), 162–172 (1987)
9. Bhadra, S., Kelkar, V.A., Brooks, F.J., Anastasio, M.A.: On hallucinations in tomographic image reconstruction. *IEEE transactions on medical imaging* **40**(11), 3249–3260 (2021)
10. Biggio, B., Corona, I., Maiorca, D., Nelson, B., Šrndić, N., Laskov, P., Giacinto, G., Roli, F.: Evasion attacks against machine learning at test time. In: Joint European conference on machine learning and knowledge discovery in databases. pp. 387–402. Springer (2013)
11. Biggio, B., Roli, F.: Wild patterns: Ten years after the rise of adversarial machine learning. In: Proceedings of the 2018 ACM SIGSAC Conference on Computer and Communications Security. pp. 2154–2156 (2018)

12. Block, K.T., Uecker, M., Frahm, J.: Undersampled radial MRI with multiple coils. Iterative image reconstruction using a total variation constraint. *Magnetic Resonance in Medicine: An Official Journal of the International Society for Magnetic Resonance in Medicine* **57**(6), 1086–1098 (2007)
13. Carlini, N., Wagner, D.: Adversarial examples are not easily detected: Bypassing ten detection methods. In: *Proceedings of the 10th ACM workshop on artificial intelligence and security*. pp. 3–14 (2017)
14. Chambolle, A., Caselles, V., Cremers, D., Novaga, M., Pock, T., et al.: An introduction to total variation for image analysis. *Theoretical foundations and numerical methods for sparse recovery* **9**(263-340), 227 (2010)
15. Chattopadhyay, N., Chattopadhyay, A., Gupta, S.S., Kasper, M.: Curse of dimensionality in adversarial examples. In: *2019 International Joint Conference on Neural Networks (IJCNN)*. pp. 1–8. IEEE (2019)
16. Chen, S., Donoho, D.: Basis pursuit. In: *Proceedings of 1994 28th Asilomar Conference on Signals, Systems and Computers*. vol. 1, pp. 41–44. IEEE (1994)
17. Chen, Y., Caramanis, C., Mannor, S.: Robust sparse regression under adversarial corruption. In: *International conference on machine learning*. pp. 774–782. PMLR (2013)
18. Cheng, K., Calivá, F., Shah, R., Han, M., Majumdar, S., Pedoia, V.: Addressing The False Negative Problem of Deep Learning MRI Reconstruction Models by Adversarial Attacks and Robust Training. In: Arbel, T., Ben Ayed, I., de Bruijne, M., Descoteaux, M., Lombaert, H., Pal, C. (eds.) *Proceedings of the Third Conference on Medical Imaging with Deep Learning*. *Proceedings of Machine Learning Research*, vol. 121, pp. 121–135. PMLR (06–08 Jul 2020), <https://proceedings.mlr.press/v121/cheng20a.html>
19. Cohen, J., Rosenfeld, E., Kolter, Z.: Certified adversarial robustness via randomized smoothing. In: *international conference on machine learning*. pp. 1310–1320. PMLR (2019)
20. Colbrook, M.J., Antun, V., Hansen, A.C.: The difficulty of computing stable and accurate neural networks: On the barriers of deep learning and Smale’s 18th problem. *Proceedings of the National Academy of Sciences* **119**(12), e2107151119 (2022)
21. Costa, J.C., Roxo, T., Proença, H., Inacio, P.R.M.: How deep learning sees the world: A survey on adversarial attacks & defenses. *IEEE Access* **12**, 61113–61136 (2024)
22. Darestani, M.Z., Chaudhari, A.S., Heckel, R.: Measuring robustness in deep learning based compressive sensing. In: *International Conference on Machine Learning*. pp. 2433–2444. PMLR (2021)
23. Dong, J., Chen, J., Xie, X., Lai, J., Chen, H.: Survey on adversarial attack and defense for medical image analysis: Methods and challenges. *ACM Computing Surveys* **57**(3), 1–38 (2024)
24. Farquhar, S., Kossen, J., Kuhn, L., Gal, Y.: Detecting hallucinations in large language models using semantic entropy. *Nature* **630**(8017), 625–630 (2024)
25. Foucart, S., Rauhut, H.: *A Mathematical Introduction to Compressive Sensing*. Springer New York (2013). <https://doi.org/10.1007/978-0-8176-4948-7>, <http://dx.doi.org/10.1007/978-0-8176-4948-7>
26. Genzel, M., Macdonald, J., März, M.: Solving inverse problems with deep neural networks – robustness included? *IEEE transactions on pattern analysis and machine intelligence* **45**(1), 1119–1134 (2022)
27. Gilmer, J., Metz, L., Faghri, F., Schoenholz, S., Raghu, M., Wattenberg, M., Goodfellow, I.: Adversarial spheres (2018), <https://openreview.net/forum?id=SyUkxxZ0b>

28. Gottschling, N.M., Antun, V., Hansen, A.C., Adcock, B.: The troublesome kernel: On hallucinations, no free lunches, and the accuracy-stability tradeoff in inverse problems. *SIAM Review* **67**(1), 73–104 (2025)
29. Hammernik, K., Klatzer, T., Kobler, E., Recht, M.P., Sodickson, D.K., Pock, T., Knoll, F.: Learning a variational network for reconstruction of accelerated MRI data. *Magnetic resonance in medicine* **79**(6), 3055–3071 (2018)
30. Heckel, R., Jacob, M., Chaudhari, A., Perlman, O., Shimron, E.: Deep learning for accelerated and robust MRI reconstruction: a review. *arXiv preprint arXiv:2404.15692* (2024)
31. Kaviani, S., Han, K.J., Sohn, I.: Adversarial attacks and defenses on ai in medical imaging informatics: A survey. *Expert Systems with Applications* **198**, 116815 (2022)
32. Kawata, S., Nalcioglu, O.: Constrained iterative reconstruction by the conjugate gradient method. *IEEE transactions on medical imaging* **4**(2), 65–71 (2007)
33. Kurakin, A., Goodfellow, I.J., Bengio, S.: Adversarial examples in the physical world. In: *Artificial intelligence safety and security*, pp. 99–112. Chapman and Hall/CRC (2018)
34. Lee, S., Lee, W., Park, J., Lee, J.: Towards better understanding of training certifiably robust models against adversarial examples. In: Ranzato, M., Beygelzimer, A., Dauphin, Y., Liang, P., Vaughan, J.W. (eds.) *Advances in Neural Information Processing Systems*. vol. 34, pp. 953–964. Curran Associates, Inc. (2021), https://proceedings.neurips.cc/paper_files/paper/2021/file/07c5807d0d927dcd0980f86024e5208b-Paper.pdf
35. Mao, Y., Müller, M., Fischer, M., Vechev, M.: Connecting certified and adversarial training. *Advances in Neural Information Processing Systems* **36**, 73422–73440 (2023)
36. Morshuis, J.N., Gatidis, S., Hein, M., Baumgartner, C.F.: Adversarial robustness of MR image reconstruction under realistic perturbations. In: *International Workshop on Machine Learning for Medical Image Reconstruction*. pp. 24–33. Springer (2022)
37. Muckley, M.J., Riemenschneider, B., Radmanesh, A., Kim, S., Jeong, G., Ko, J., Jun, Y., Shin, H., Hwang, D., Mostapha, M., et al.: State-of-the-art machine learning MRI reconstruction in 2020: Results of the second fastMRI challenge. *arXiv preprint arXiv:2012.06318* **2**(6) (2020)
38. Muckley, M.J., Riemenschneider, B., Radmanesh, A., Kim, S., Jeong, G., Ko, J., Jun, Y., Shin, H., Hwang, D., Mostapha, M., et al.: Results of the 2020 fastMRI challenge for machine learning MR image reconstruction. *IEEE transactions on medical imaging* **40**(9), 2306–2317 (2021)
39. Peck, J., Goossens, B.: Robust width: A lightweight and certifiable adversarial defense. *arXiv preprint arXiv:2405.15971* (2024)
40. Peck, J., Goossens, B., Saeys, Y.: An introduction to adversarially robust deep learning. *IEEE Transactions on Pattern Analysis and Machine Intelligence* (2023)
41. Ribes, A., Schmitt, F.: Linear inverse problems in imaging. *IEEE Signal Processing Magazine* **25**(4), 84–99 (2008)
42. Roemer, P.B., Edelstein, W.A., Hayes, C.E., Souza, S.P., Mueller, O.M.: The NMR phased array. *Magnetic resonance in medicine* **16**(2), 192–225 (1990)
43. Ronneberger, O., Fischer, P., Brox, T.: U-net: Convolutional networks for biomedical image segmentation. In: *International Conference on Medical image computing and computer-assisted intervention*. pp. 234–241. Springer (2015)
44. Salman, H., Sun, M., Yang, G., Kapoor, A., Kolter, J.Z.: Denoised smoothing: A provable defense for pretrained classifiers. *Advances in Neural Information Processing Systems* **33**, 21945–21957 (2020)

45. Sidky, E.Y., Lorente, I., Brankov, J.G., Pan, X.: Do CNNs solve the CT inverse problem? *IEEE Transactions on Biomedical Engineering* **68**(6), 1799–1810 (2020)
46. Sriram, A., Zbontar, J., Murrell, T., Defazio, A., Zitnick, C.L., Yakubova, N., Knoll, F., Johnson, P.: End-to-end variational networks for accelerated mri reconstruction. In: Martel, A.L., Abolmaesumi, P., Stoyanov, D., Mateus, D., Zuluaga, M.A., Zhou, S.K., Racoceanu, D., Joskowicz, L. (eds.) *Medical Image Computing and Computer Assisted Intervention – MICCAI 2020*. pp. 64–73. Springer International Publishing, Cham (2020)
47. Sulam, J., Muthukumar, R., Arora, R.: Adversarial robustness of supervised sparse coding. *Advances in neural information processing systems* **33**, 2110–2121 (2020)
48. Szegedy, C., Zaremba, W., Sutskever, I., Bruna, J., Erhan, D., Goodfellow, I., Fergus, R.: Intriguing properties of neural networks. *arXiv preprint arXiv:1312.6199* (2013)
49. Torrence, C., Compo, G.P.: A practical guide to wavelet analysis. *Bulletin of the American Meteorological society* **79**(1), 61–78 (1998)
50. Tramer, F., Carlini, N., Brendel, W., Madry, A.: On adaptive attacks to adversarial example defenses. *Advances in neural information processing systems* **33**, 1633–1645 (2020)
51. Tropp, J.A., Wright, S.J.: Computational methods for sparse solution of linear inverse problems. *Proceedings of the IEEE* **98**(6), 948–958 (2010)
52. Uecker, M., Lai, P., Murphy, M.J., Virtue, P., Elad, M., Pauly, J.M., Vasanawala, S.S., Lustig, M.: ESPIRiT—an eigenvalue approach to autocalibrating parallel MRI: where SENSE meets GRAPPA. *Magnetic resonance in medicine* **71**(3), 990–1001 (2014)
53. Wang, Z., Bovik, A.C., Sheikh, H.R., Simoncelli, E.P.: Image quality assessment: from error visibility to structural similarity. *IEEE transactions on image processing* **13**(4), 600–612 (2004)
54. Winograd, S.: On computing the discrete Fourier transform. *Mathematics of computation* **32**(141), 175–199 (1978)
55. Xu, Z., Jain, S., Kankanhalli, M.S.: Hallucination is inevitable: An innate limitation of large language models. *CoRR* **abs/2401.11817** (2024), <https://doi.org/10.48550/arXiv.2401.11817>
56. Zbontar, J., Knoll, F., Sriram, A., Murrell, T., Huang, Z., Muckley, M.J., Defazio, A., Stern, R., Johnson, P., Bruno, M., et al.: fastMRI: An open dataset and benchmarks for accelerated MRI. *arXiv preprint arXiv:1811.08839* (2018)
57. Zhang, M., Gu, S., Shi, Y.: The use of deep learning methods in low-dose computed tomography image reconstruction: a systematic review. *Complex & intelligent systems* **8**(6), 5545–5561 (2022)

A Pseudocode of the attack

Algorithm A.1 Masked Iterative FGSM Attack

F Reconstruction map.

\mathbf{z} Raw k -space input sample.

\mathbf{y}_t Target reconstruction with artificial detail.

\mathbf{m} Binary mask delineating the target region.

ε Maximum perturbation magnitude.

α Step size per iteration.

T Number of iterations.

```

1: function MASKEDITERATIVEFGSM( $F, \mathbf{z}, \mathbf{y}_t, \mathbf{m}, \varepsilon, \alpha, T$ )
2:    $\mathbf{y}_0 \leftarrow F(\mathbf{z})$  ▷ Obtain clean reconstruction
3:    $\boldsymbol{\delta} \sim \text{Unif}(-\varepsilon, \varepsilon)$  ▷ Random initial perturbation
4:    $\boldsymbol{\delta}^* \leftarrow \boldsymbol{\delta}$  ▷ Initial best perturbation
5:    $L_{\min} \leftarrow +\infty$  ▷ Initial best loss value
   // Optimization loop
6:   for  $t \leftarrow 1$  to  $T$  do
   // Compute perturbed sample
7:      $\mathbf{z}_{\text{adv}} \leftarrow \text{clip}(\Re(\mathbf{z}) + \boldsymbol{\delta}, 0, 1) + \Im(\mathbf{z})$ 
   // Compute loss
8:      $L_1 \leftarrow \|\mathbf{m} \odot (F(\mathbf{z}_{\text{adv}}) - \mathbf{y}_t)\|_2^2$ 
9:      $L_2 \leftarrow \|(1 - \mathbf{m}) \odot (F(\mathbf{z}_{\text{adv}}) - F(\mathbf{z}))\|_2^2$ 
10:     $L \leftarrow \frac{L_1}{\|\mathbf{m}\|_1} + \frac{L_2}{\|1 - \mathbf{m}\|_1}$ 
   // Keep track of the best perturbation
11:    if  $L < L_{\min}$  then
12:       $\boldsymbol{\delta}^* \leftarrow \boldsymbol{\delta}$ 
13:       $L_{\min} \leftarrow L$ 
14:    end if
   // Compute update
15:     $\boldsymbol{\delta} \leftarrow \boldsymbol{\delta} - \alpha \cdot \text{sign}(\nabla_{\boldsymbol{\delta}} L)$ 
16:     $\boldsymbol{\delta} \leftarrow \text{clip}(\boldsymbol{\delta}, -\varepsilon, \varepsilon)$ 
17:  end for
18:  return  $\boldsymbol{\delta}^*$ 
19: end function

```

B Qualitative assessment of the attack

For a qualitative assessment of the results, we show some examples in figure B.1 for the UNet model and figure B.2 for the E2E-VarNet model of reconstructions where the attack was successful. These figures are structured as 2x2 panels of images where the first row displays the original and perturbed input samples and the second row displays the corresponding model-based reconstructions. Areas which we believe contain hallucinatory structures are highlighted in red.

We notice from figures B.1a and B.1b that the multi-coil images seem to be more vulnerable than the single-coil ones, in the sense that the resulting distortions are more severe for multi-coil data. The generated perturbations also seem easier to spot for single-coil data. This may be explained by the fact that perturbations in the multi-coil images can be more “spread out” across the coils, whereas with single-coil data this is not possible. This is consistent with the observation that vulnerability to adversarial examples increases with data dimensionality [15, 27]. Although we cannot compare to single-coil data for the E2E-VarNet, we do notice large distortions in figure B.2a as well that go far beyond the boundaries of our inserted detail. On the multi-coil brain data, the hallucinations seem less severe for both models compared to the knee data, but the distortions can still be significant as they tend to resemble non-existent sulci. For knee images, the distortions appear to substantially change the structure of the knee joint, especially on multi-coil data.

We conclude that the adversarially perturbed samples can lead to realistic reconstructions which exhibit biologically plausible distortions that could mislead expert interpretation, and that the insertion of the artificial detail will often cause further distortion beyond the original target region. For both models, this is especially apparent in the multicoil knee data, where the shape of the knee joint tends to change significantly when the detail is inserted.

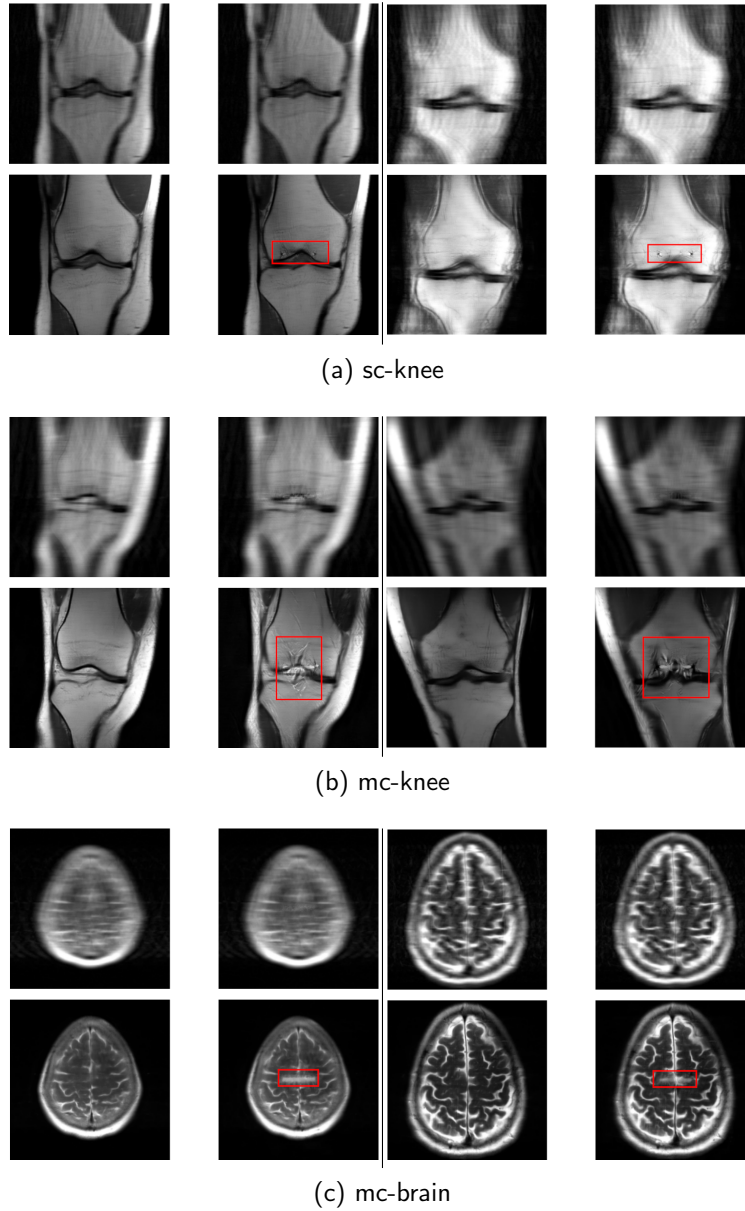


Fig. B.1. Examples of successful attacks on the UNet model. For each data set, the first row displays the input samples (original on the left, adversarially perturbed on the right) and the second row displays the corresponding outputs. The generated hallucinations are annotated in red.

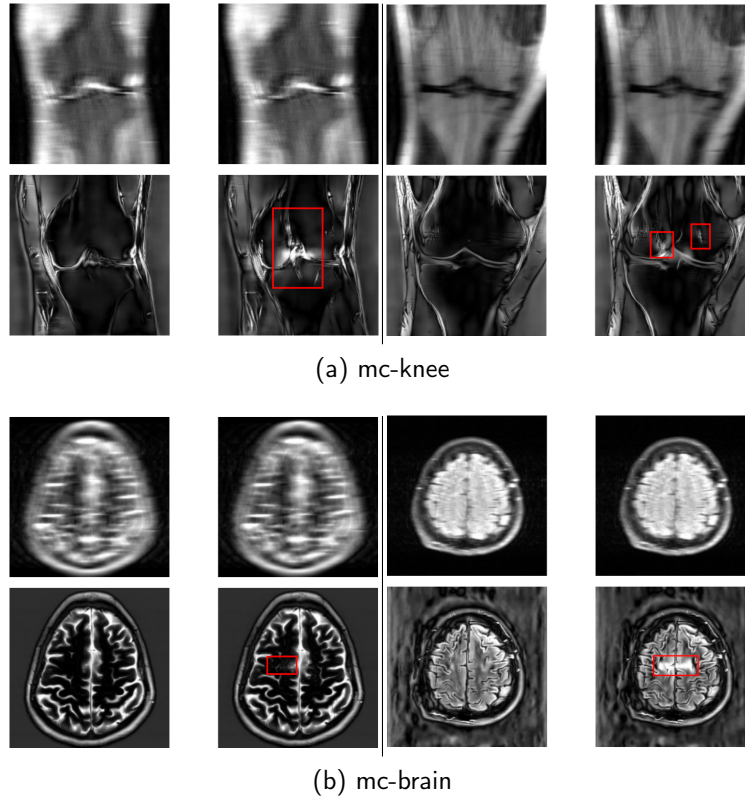


Fig. B.2. Examples of successful attacks on the E2E-VarNet model. For each data set, the first row displays the input samples (original on the left, adversarially perturbed on the right) and the second row displays the corresponding outputs. The generated hallucinations are annotated in red.